Numerical simulations of localization of electromagnetic waves in two- and three-dimensional disordered media

Ameneh Sheikhan,[1] M. Reza Rahimi Tabar,[1,2] and Muhammad Sahimi[3,*]
[1]*Department of Physics, Sharif University of Technology, Tehran 11155-9161, Iran*
[2]*Institute of Physics, Carl von Ossietzky University, D-26111 Oldenburg, Germany*
[3]*Mork Family Department of Chemical Engineering & Materials Science, University of Southern California, Los Angeles, California 90089-1211, USA*

(Received 9 December 2008; revised manuscript received 18 June 2009; published 28 July 2009)

Localization of electromagnetic waves in two-dimensional (2D) and three-dimensional (3D) media with random permittivities is studied by numerical simulations of the Maxwell's equations. Using the transfer-matrix method, the minimum positive Lyapunov exponent γ_m of the model is computed, the inverse of which is the localization length. Finite-size scaling analysis of γ_m is carried out in order to check the localization-delocalization transition in 2D and 3D. We show that in 3D disordered media γ_m exhibits two distinct types of frequency dependence over two frequency ranges, hence indicating the existence of a localization-delocalization transition at a critical frequency ω_c. The critical exponent ν of the localization length in 3D is estimated to be, $\nu \simeq 1.57 \pm 0.07$. At the transition point in the 3D media, the distribution function of the level spacings is *independent* of the system size, and is represented well by the semi-Poisson distribution. The 2D model can be mapped onto the 2D Anderson model and, hence, there is no localization-delocalization transition.

DOI: 10.1103/PhysRevB.80.035130 PACS number(s): 71.23.An, 71.55.Jv, 63.20.Pw

I. INTRODUCTION

Wave propagation in heterogeneous media is a fundamental phenomenon of great scientific and practical interest, and has been studied for a long time.[1] Many years of research have established rigorously that, in one-dimensional (1D) media with diagonal disorder and short-range correlations, even infinitesimally small disorder suffices for localizing the wave function, irrespective of the energy.[2,3] Thus, envelope of the wave function $\psi(r)$ for the localized states decays exponentially at large distances r from the domain's center, $\psi(r) \sim \exp[-r/\xi(E)]$, with $\xi(E)$ being the localization length at energy level E. Some rigorous results have also been derived for higher-dimensional disordered media.[1]

In this paper we study propagation and localization of electromagnetic waves in disordered media. What we study is directly relevant to, among other phenomena, propagation of light through such disordered media as fog and clouds, as well as propagation of electromagnetic waves through stellar atmospheres and interstellar clouds, all of which are subjects of current interest. A study of diffusive wave propagation was first undertaken by astrophysicists,[4,5] with the goal of understanding how radiation generated at the center of stars is affected as it traverses through the interstellar clouds. At the same time, the question of whether light can be localized in disordered media,[6] in addition to be of much current interest, has still not been addressed completely. Unlike the problem of electron localization in disordered materials, which is of interacting quantum type, electromagnetic waves are noninteracting, even at the quantum level and, therefore, their propagation provides a suitable framework for realizing the properties of the Anderson model of localization.[7] In fact, the first observations of strong[8–11] and weak localization[12–15] motivated much research on the question of light localization,[16] as a way of determining the mobility edge.[17–19]

The standard method of numerical analysis of wave propagation in disordered media and estimating the localization length, in spatial dimensions two and three (where there are not many known exact results), is the transfer-matrix (TM) method.[20] In the TM method one fixes the frequency of the wave or the energy level of the incident particles and computes the Lyapunov exponent or its inverse, the localization length. In the limit of weak disorder, however, obtaining numerically convergent and accurate results by the TM method requires intensive computations.

Using the TM method, we study in this paper the localization properties of electromagnetic waves in disordered media over a range of the frequencies. Then, utilizing the finite-size scaling method we study whether there is a localization-delocalization transition in such disordered media. We also study the statistics of the energy levels.[21,22] In addition, we compute the number variance, a long-range correlator that represents the variance of the number of the eigenfrequencies in a given interval. The number variance helps us identify which frequencies are localized or delocalized.

Depending on the symmetry of the Hamiltonian that one studies, one may have distinct symmetry classes. For a system of noninteracting electrons moving in a random potential, there are three well-known symmetry classes, namely, the Gaussian orthogonal ensemble (GOE), the Gaussian unitary ensemble, and the Gaussian symplectic ensemble. These represent random-matrix ensembles that are generally called the Wigner-Dyson statistics.[23] In this paper we study the level statistic of electromagnetic waves in disordered media, in order to not only identify its universality class, but also check the existence of the localization-delocalization transition as the intensity of the disorder increases. We show below that the behavior of electromagnetic waves in the disordered media that we study belongs to the GOE universality

class (see also[24,25] about the new development of wave localization in random media).

The rest of this paper is organized as follows. In the next section the model that we study is introduced, and the governing equations for propagation of electromagnetic waves are outlined. How the TM method is implemented is described in Sec. III, while the TM results are described in Sec. IV. The computations of the density of state and the mobility edge are described in Sec. V. In Sec. VI the statistics of the energy levels are investigated. The results and conclusions are summarized in the last section.

II. MODEL AND GOVERNING EQUATIONS

We consider a medium with a random (white noise) distribution of the dielectric constants. Maxwell's dynamical equations are utilized for describing the propagation of electromagnetic waves. Discretizing the governing equations enables us to calculate the Hamiltonian matrix, and to carry out the numerical simulations. The dynamical Maxwell's equations are given by

$$\nabla \times \mathbf{H} = \partial \mathbf{D}/\partial t,$$

$$\nabla \times \mathbf{E} = -\partial \mathbf{B}/\partial t. \tag{1}$$

Here, $\mathbf{D}=\epsilon\mathbf{E}$ and, $\mathbf{H}=\mu^{-1}\mathbf{B}$, where $\mathbf{E}$ and $\mathbf{B}$ are the electric and magnetic fields, respectively. The permittivity field $\epsilon(\mathbf{x})$ is considered as a random variable, given by, $\epsilon(\mathbf{x})=\bar{\epsilon}+\eta(\mathbf{x})=k\epsilon_0+\eta(\mathbf{x})$, with its mean being, $\bar{\epsilon}=\langle\epsilon(\mathbf{x})\rangle$, where $\eta(\mathbf{x})$ is a white noise with variance W^2, i.e., $\langle\eta(\mathbf{x}_1)\eta(\mathbf{x}_2)\rangle=W^2\delta(\mathbf{x}_1-\mathbf{x}_2)$.

Let us rescale the variables by writing, $x'=x/x_0$, $t'=ct/(x_0\sqrt{k})$, $E'=E/E_0$, $B'=cB/(E_0\sqrt{k})$, and $\eta'(x')=\eta(x)/\bar{\epsilon}$, which then yield the following dimensionless equations:

$$\nabla' \times \mathbf{B}' = [1+\eta'(x')]\,\partial\mathbf{E}'/\partial t',$$

$$\nabla' \times \mathbf{E}' = -\partial\mathbf{B}'/\partial t'. \tag{2}$$

The variance of W^2 is rescaled as, $W'^2=W^2/(\bar{\epsilon}^2x_0)$, so that, $\langle\eta'(\mathbf{x}_1')\eta'(\mathbf{x}_2')\rangle=(W'^2/\Delta')\delta_{\mathbf{x}_1',\mathbf{x}_2'}=\sigma^2\delta_{\mathbf{x}_1',\mathbf{x}_2'}$, where Δ' is the lattice spacing of the rescaled system. Thus, the noise η' is characterized by its width, $\sigma=(W'^2/\Delta')^{1/2}=W/W_0$, with, $W_0^2=\bar{\epsilon}^2x_0\Delta'=\bar{\epsilon}^2\Delta$.

To carry out the computations we use Yee's computational grid, which is commonly used in the numerical simulations of electromagnetic phenomena.[26,27] For simplicity, the indices (i,j,k) are used to represent the elementary cubic block of the grid; see Fig. 1. We then derive the discretized forms of the electromagnetic waves equations at frequency ω, in terms of such indices by using the finite-difference discretization, which enables us to formulate the computations as an eigenvalue problem. If we consider a vector, $\mathbf{\Psi}=(\mathbf{E},\mathbf{B})$, the components of which are the (numerical values of the) electric and magnetic fields in the entire computational grid, the eigenvalue problem is expressed by

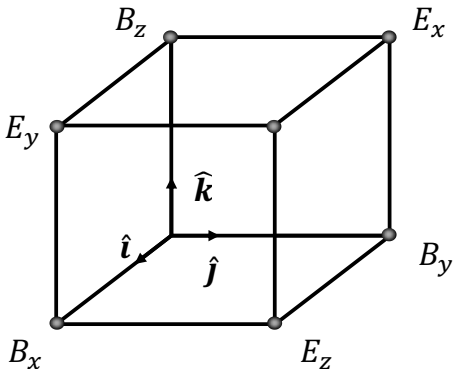

FIG. 1. The elementary cell in the computational grid known as the Yee's mesh. The sides of the cubic block have length $\frac{1}{2}\Delta$.

$$\sum_\beta H_{\alpha\beta}\Psi_\beta = \omega\Psi_\alpha, \tag{3}$$

where we have considered the electromagnetic field in the form, $\mathbf{\Psi}(\mathbf{x},t)=\mathbf{\Psi}(\mathbf{x})\exp(i\omega t)$.

In the 2D systems the function $\mathbf{\Psi}$ depends only on (y,z). This leads to dividing Maxwell's equations into two independent parts. One part contains the governing equations for the fields (E_x,B_y,B_z) (the s-polarized wave), while the second part contains the governing equations for the fields (B_x,E_y,E_z) (the p-polarized wave). Therefore, for the 2D media the Hamiltonian H reduces to two block-diagonal matrices such that each block is investigated separately, with no coupling between the two polarizations.

III. TRANSFER-MATRIX METHOD

Numerical simulations were carried out for 2D strips and 3D bars. Using the TM method, we computed the smallest positive Lyapunov exponent γ_m, which represents the inverse of the localization length. The discretized equation for, for example, the field B_x is given by

$$\begin{aligned} B_x(i,j,k+1) = &-\frac{1}{\omega}[E_y(i+1,j,k)-E_y(i,j,k)-E_x(i+1,j,k) \\ &+E_x(i+1,j-1,k)]+\frac{1}{\omega}[E_y(i,j,k)-E_y(i \\ &-1,j,k)-E_x(i,j,k)+E_x(i,j-1,k)] \\ &+\Delta\omega\mu\epsilon(i,j,k)E_y(i,j,k)+B_x(i,j,k). \end{aligned} \tag{4}$$

For convenience, all the primes have been omitted. The derivatives are accurate to order Δ^3. In the numerical simulations we set $\Delta=1$ and distributed uniformly the random variable η, representing the disorder, in the interval $[-\sigma,\sigma]$. To formulate the TM computations the equations for the fields $(\mathbf{E},\mathbf{B})$ are written in the following form:

$$\begin{pmatrix} \tilde{\mathbf{E}}_x \\ \tilde{\mathbf{E}}_y \\ \tilde{\mathbf{B}}_x \\ \tilde{\mathbf{B}}_y \end{pmatrix}_{k+1} = \mathbf{T}_k \begin{pmatrix} \tilde{\mathbf{E}}_x \\ \tilde{\mathbf{E}}_y \\ \tilde{\mathbf{B}}_x \\ \tilde{\mathbf{B}}_y \end{pmatrix}_k, \tag{5}$$

where $\mathbf{T}_k$ is the TM for the slice k, and $(\tilde{\mathbf{E}}_x)_k$ the vector that contains the values of E_x in that slice, and so on. Thus,

TABLE I. The rescaled Lyapunov exponents $M\gamma_\alpha$ of the 2D model and the corresponding estimated errors. α is the index number of the sorted Lyapunov exponents γ that varies from $1M$ to $2M$. Here, we used strips of width $M=10$ and length $L=10^6$ with periodic boundary conditions, with the disorder intensity $\sigma=0.99$ and frequency $\omega=2$. The errors were estimated by the rate of the convergence of γ_α during the iterations (Ref. 28). Only the absolute values of the smallest γ_α are presented.

α	$M\gamma_\alpha$	Error	α	$M\gamma_\alpha$	Error
10	3.854360	0.006162	11	−3.854369	0.006162
9	6.518471	0.005704	12	−6.518461	0.005704
8	8.709773	0.005329	13	−8.709799	0.005329
7	10.613867	0.005002	14	−10.613855	0.005003
6	12.295612	0.004690	15	−12.295623	0.004690
5	13.791556	0.004405	16	−13.791550	0.004405

through numerical simulations the values of B_x and B_y in the slice $k+1$ are computed using values of E_x, E_y, B_x, and B_y in the slice k, while values of E_x and E_y in the slice $k+1$ are calculated knowing E_x and E_y in the slice k and B_x and B_y in the slice $k+1$, which we compute in the previous step.

In the 2D case, the transfer-matrix T is, similar to its Hamiltonian H, block diagonal. One block transfers the vector $(\tilde{\mathbf{E}}_x, \tilde{\mathbf{B}}_y)_k^t$ to $(\tilde{\mathbf{E}}_x, \tilde{\mathbf{B}}_y)_{k+1}^t$, where t denotes the transpose operation, and another vector transfers $(\tilde{\mathbf{E}}_y, \tilde{\mathbf{B}}_x)_k^t$ to vector $(\tilde{\mathbf{E}}_y, \tilde{\mathbf{B}}_x)_{k+1}^t$. The two vectors can be investigated separately.

The disordered medium is represented by $M \times L$ strips (in 2D) and $M \times M \times L$ bars (in 3D), with periodic boundary conditions (PBCs), where M is the width and L the longitudinal length. The Lyapunov exponents are the logarithm of the eigenvalues of the matrix $(\mathbf{T}\mathbf{T}^t)^{1/2L}$, and, $\mathbf{T}=\Pi_{k=1}^{L}\mathbf{T}_k$. The Oseledec theorem[20] states that, in the limit $L\to\infty$, all the Lyapunov exponents γ_α of the matrix $\mathbf{T}$ follow the Gaussian distribution with a variance proportional to the mean value. Thus, by specifying the initial values of the fields $\mathbf{E}$ and $\mathbf{B}$ in the first lines of the strips (in 2D) and the first planes of the bars (in 3D), we compute the fields after traversing the length L by multiplying all the TMs. In the TM method the Lyapunov exponent of the electromagnetic fields indicates that these fields decay exponentially in the transfer length L by the localization length ξ, which is the inverse of Lyapunov exponent and, thus, the intensity of electromagnetic waves also decays exponentially.

The number N of the Lyapunov exponents are, $N=2M$ in 2D and $N=4M^2$ in 3D media. The simulations begin by N orthogonal initial vectors, and are carried out using the Gram-Schmidt (GS) orthogonalization after every two steps of the TM iterations. The reason for the use of the GS orthogonalization is that, after some iterations the directions of all the vectors change to the direction of the vector that corresponds to the *largest* Lyapunov exponent. The orthogonalization procedure enables us to determine the smallest (positive) Lyapunov exponents. The iterations are continued until we achieve an acceptable relative accuracy[28] for the rescaled variable, $\Lambda^{-1}=\gamma_m/M$.

IV. RESULTS FOR THE LOCALIZATION LENGTH

Let us consider, first, the 2D disordered media. In our simulation we considered the *s*-polarized wave. The Maxwell equations reduce to

$$-[1+\eta(y,z)]\omega^2 E_x(y,z) = \nabla^2 E_x(y,z). \tag{6}$$

Its discretized form is given by

$$-[1+\eta(j,k)]\omega^2 E_x(j,k) = E_x(j+1,k) + E_x(j-1,k) - 2E_x(j,k) + E_x(j,k+1) + E_x(j,k-1) - 2E_x(j,k). \tag{7}$$

The computed Lyapunov exponents γ_m are presented in Table I for $\omega=2$. They occur in pairs $(-\gamma_\alpha, \gamma_\alpha)$, which indicates the symplectic symmetry of the TMs. The inset of Fig. 2 presents the dependence of Λ^{-1} on the frequency for several widths M of the 2D strips with the PBCs in the transverse direction. There are some peaks that correspond precisely to the frequencies ω_n, with $\omega_n^2=2-2\cos(2n\pi/M)$ for the PBCs and, $\omega_n^2=2-2\cos[n\pi/(M+1)]$ for fixed boundary conditions (FBCs). The oscillating behavior is produced by the internal band edges, corresponding to some eigenmodes of the Hamiltonian in one slice of the ordered medium.[29] The peaks disappear by increasing the intensity of the disorder. Figure 3 presents the results for a 2D strip of width $M=8$, with the FBCs and the disorder intensity $\sigma=0.5$, which is smaller than that for Fig. 2. When the FBCs are used, there is a minimum allowed frequency $\omega_{\min}$ for the medium without

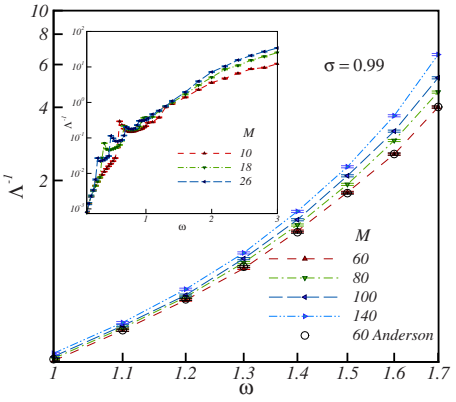

FIG. 2. (Color online) Logarithmic plot of the rescaled Lyapunov exponent Λ^{-1} versus frequency of *s*-polarized wave for several widths M of the 2D strips. The circle symbols are for Anderson model for comparison. The inset shows the logarithmic-linear plot of Λ^{-1} for different values of strip width M.

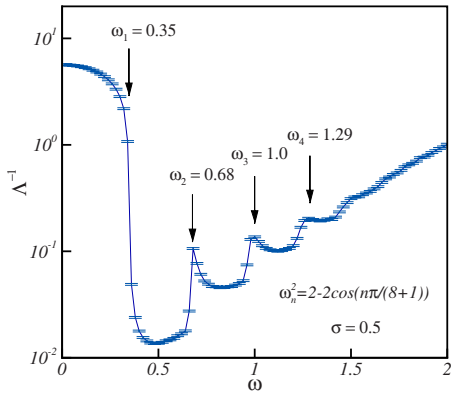

FIG. 3. (Color online) Dependence of the rescaled Lyapunov exponent Λ^{-1} on the frequency for a 2D strip with free boundary conditions, width $M=8$, and intensity of disorder σ. The peaks are sharp in the weak disorder regime.

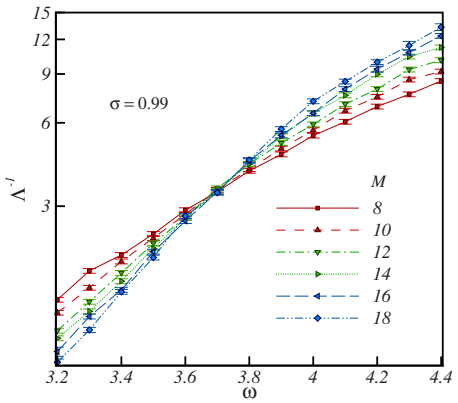

FIG. 4. (Color online) Dependence of the rescaled Lyapunov exponent Λ^{-1} on the frequency for several widths M of the 3D bars. There is a critical frequency $\omega_c \simeq 3.7 \pm 0.1$ at which the Lyapunov exponent remains unchanged by increasing the size M.

disorder, $\omega_{\min}=\omega_1 \simeq 0.35$ (for $M=8$), for which the Lyapunov exponent is not small for the frequencies $\omega < \omega_{\min}$. As the width M increases, the frequency ω_1 vanishes.

The main part of Fig. 2 presents the rescaled Lyapunov exponent for larger widths of strip. As the inset indicates, increasing the width of the strip also increases the rescaled Lyapunov exponent Λ^{-1}. Such a behavior indicates that all such frequencies are localized for the disorder strength $\sigma = 0.99$. For very small σ and ω, the numerical convergence of γ_m, as evaluated by the TM method, is very slow and accurate results are obtained by many more iterations. We carried out similar simulations for the p-polarized waves and found the behavior of the Lyapunov exponent to be similar to that of the s-polarized wave.

According to Eq. (7) the model in 2D can be mapped onto the Anderson model by the transformations, $E=4-\omega^2$, $V(j,k)=\omega^2\eta(j,k)$, and thus, $\sigma_V=\omega^2\sigma$, where E is energy, V is the random potential energy of Anderson model at node (j,k). The variance σ_V is its disorder strength. The positivity of $\epsilon(x)$ implies imposes some restriction on the variance of the disorder, i.e., $\sigma<1$. For a given frequency and intensity of the disorder in Eq. (6), there is a state in the 2D Anderson model which we know is localized. Therefore, all the states are localized for the s-polarized wave except for, $\omega=0$, with their equivalent in the Anderson model being, $E=4$ and $\sigma_V=0$. To make a comparison between the 2D Anderson model and s-polarized wave, we also calculated the rescaled Lyapunov exponent of the Anderson model. As shown in Fig. 2 (shown with circles) the two model have the same rescaled Lyapunov exponent. This means that the s-polarized wave in 2D random media does not have a localization-delocalization transition.

Figure 4 depicts the dependence of the rescaled Lyapunov exponent on the frequency for several widths of the 3D bar, with the strength of the disorder being, $\sigma=0.99$. In 3D, one obtains a distinct behavior for Λ^{-1} by increasing the width M of the bar, as the frequency is varied. The scaling hypothesis[30,31] states that, there is a unique scaling function F such that one has a scaling parameter $\xi(\omega)$ and a scaling form, $\Lambda^{-1}(\omega)=F[M/\xi(\omega)]$. The dependence of ξ on the frequency was computed by rescaling Λ^{-1} to determine the critical frequency ω_c at which the behavior changes.

Figure 5 presents a one-parameter scaling representation of Λ^{-1}. In the 3D bars one obtains a collapse of the numerical results for the Lyapunov exponent onto two scaling curves, obtained for several widths M. The presence of the two branches is the signature of the existence of the localization-delocalization transition. The lower and upper branches correspond to the delocalized and localized states, respectively. The inset in Fig. 5 presents the frequency dependence of ξ, treated as the scaling parameter. The localization ξ diverges at the critical frequency ω_c. We found that, $\omega_c=3.7\pm0.1$, for the disorder intensity $\sigma=0.99$. The localization length exponent ν defined by, $\xi \sim (\omega-\omega_c)^{-\nu}$, is determined by fitting the numerical data to the expansion of the one-parameter scaling function of the rescaled Lyapunov exponent,[32,33]

$$\Lambda^{-1} = F(\chi M^{1/\nu}) = \sum_{i=0}^{n} a_i \chi^i M^{i/\nu}, \tag{8}$$

where $\chi=\xi^{-\nu}$ and a_0 is the critical value of Λ^{-1}. Without loss of generality, the coefficient a_1 is set to be unity in Eq. (8).

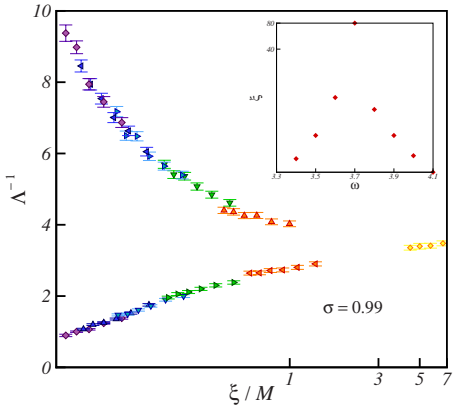

FIG. 5. (Color online) Linear-logarithmic plot of the rescaled Lyapunov exponent Λ^{-1} of the 3D bars with disorder intensity σ, as a function of $\xi(\omega)/M$. The lower and upper branches correspond to the *delocalized* and *localized* states, respectively. The inset shows the logarithm of the scaling parameter ξ as a function of ω.

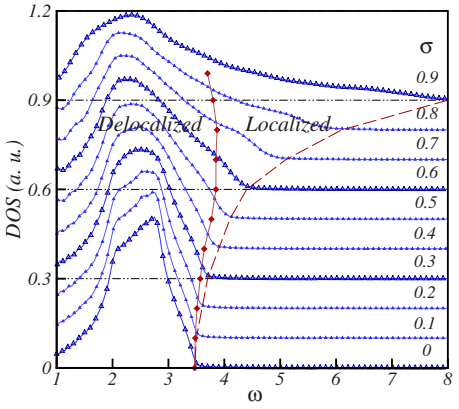

FIG. 6. (Color online) The density of states and mobility edge. The triangular dots show the DOS for several disorder intensities σ, while the diamond dots indicate the mobility edge for each σ, which was calculated by the TM method. The long-dashed lines represent the maximum allowed frequency of the DOS for several disorder intensities. The localized and extended areas are also identified in the figure.

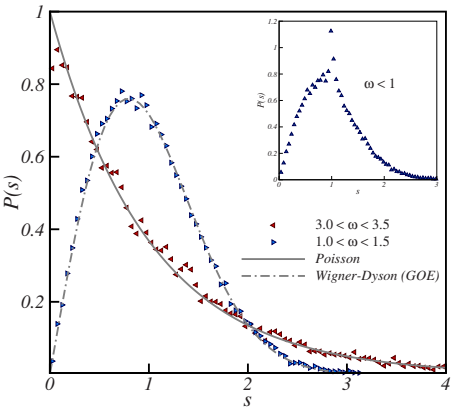

FIG. 7. (Color online) Level statistics of the 2D media of size 80^2, averaged over 200 realizations of the disorder, with the disorder parameter $\sigma=0.99$, for two frequency windows. The high frequencies results follow the Poisson distribution, whereas the intermediate frequencies are well represented by the WD distribution. The inset shows the level statistics of very low frequencies in the ballistic regime. Here, peak is seen at $s=1$.

The scaling parameter χ is then expanded as a function of the reduced frequency, $\omega_r=(\omega-\omega_c)/\omega_c$,

$$\chi=\sum_{i=1}^{m} b_i\omega_r^i. \tag{9}$$

For frequencies close to the critical frequency, we can truncate the expansion of Eqs. (8) and (9). $n=3$ and $m=2$ proved to provide accurate results. The estimated parameters and the exponent are

$$\omega_c \simeq 3.67 \pm 0.03, \quad \Lambda_c^{-1} \simeq 3.2 \pm 0.1, \quad \nu \simeq 1.57 \pm 0.07.$$

We note that the estimated critical exponent ν is the same as that of the 3D Anderson model.

V. DENSITY OF STATES AND THE MOBILITY EDGE

In 3D, one can determine the phase space of the model, i.e., determine, for a given disorder strength, the frequency interval in which the modes are localized. Let us first determine the density of state (DOS) of the model in 3D. We used the force oscillator method[34] (FOM) to calculate the DOS of the model. The FOM is an algorithm that is particularly suitable for the treating physical systems that are described by very large matrices. The scheme enables us to compute the spectral densities of both Hermitian and non-Hermitian matrices with high speed and accuracy, especially when combined with a fast time-evolution method that is based on the Chebyshev polynomial expansion.[34]

The Hamiltonian matrix introduced in Eq. (3) was used in the computations with the FOM. The Maxwell's dynamical equations, Eqs. (1), satisfy the conditions, $\nabla\cdot\mathbf{D}=0$, and $\nabla\cdot\mathbf{B}=0$, for every frequency but $\omega=0$. In Fig. 6 the DOS and the mobility edge of a 3D bar, which were calculated by TM method, are plotted for several disorder intensities. The DOS was calculated so as to determine the allowed frequencies for a given intensity of disorder, and to check whether the critical frequency ω_c is in the allowed frequency area. The states in a small part of the phase space, between the long-dashed line and the mobility edge line, are all localized. The low frequencies are the delocalized states and belong to the extended regime.

VI. LEVEL STATISTICS

We also studied the level statistic[35,36] of the models in both 2D and 3D. In what follows we described the method of the computations, after which the results are described.

A. Level-spacing distributions and number variance

To carry out the level-statistics analysis, we computed the eigenvalues of the Hamiltonian by using a numerical diagonalization technique. The level-spacing distribution $P(s)$ was calculated for a given intensity of the disorder and frequency window. Here $P(s)$ is the probability of finding two neighboring eigenvalues at a distance

$$s=\frac{\omega_{i+1}-\omega_i}{\langle\omega_{i+1}-\omega_i\rangle}.$$

The statistics of the level spacings indicate that in the localized regime, where the localization length is small compared to the medium's linear size, the wave functions have small overlaps, so that the corresponding levels are uncorrelated and follow a Poisson distribution.

The results, shown in Fig. 7, were obtained by exact diagonalization and averaging over 200 realizations of the disorder intensity with $\sigma=0.99$, using computational grids of size 80×80 (in 2D). At high frequencies the results are fitted well by the Poisson distribution, whereas the small-frequency statistics are accurately represented by the Wigner-Dyson (WD) distribution, which is in the universality class of the GOE. For very low frequencies the statistics are distinct from those described by the WD distribution. As

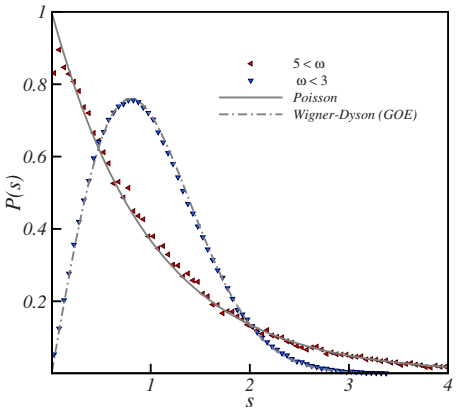

FIG. 8. (Color online) Level statistics of 3D media of size 24^3, averaged over 200 realizations of the disorder with $\sigma=0.99$, for two frequency windows. The high frequency results follow the Poisson distribution, whereas the low-frequency ones are accurately represented by the WD distribution.

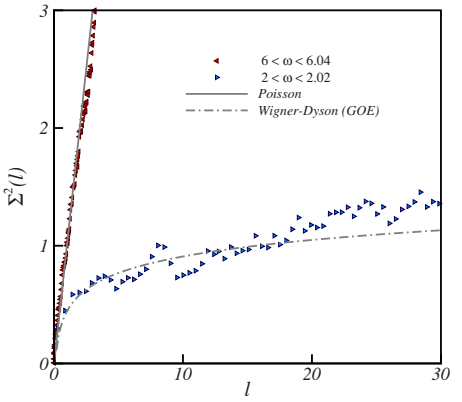

FIG. 9. (Color online) The number variance Σ^2 of the 3D media of size 24^3 for two frequency windows, averaged over 200 realizations of the disorder with $\sigma=0.99$.

is well known, in the ballistic regime the level-spacing distribution $P(s)$ approaches a delta function centered around the mean, $s=1$. Such a δ function is evident in the level statistics at very low frequencies, depicted in the inset of Fig. 7.

We note that, as described above, in the 2D disordered media the structure of the Yee's mesh gives rise to a Hamiltonian that consists of two block-diagonal matrices. Each of the two sets represents the eigenvectors of different blocks of the Hamiltonian. Each block has eigenfrequencies that have no correlations with the frequencies of the other block. However very low frequencies do not still follow the GOE distribution because of finite-size effect they are in the ballistic regime.

Figure 8 presents the frequency dependence of the level statistics for grids of size $24\times24\times24$ with $\sigma=0.99$, and the same number of realizations. The results at high frequencies are fitted well by the Poisson distribution, whereas the low-frequency statistics are represented accurately by the WD distribution (which is in the universality class of the GOE). These results are similar to those for the 2D systems. In the next section, however, we investigate the finite-size scaling of the distributions in the 2D and 3D media, in order to confirm the localization-delocalization transition.

We also computed and studied a long-range correlators, namely, the number variance,[23] $\Sigma^2(l)=\langle N(l)\rangle^2-\langle N^2(l)\rangle$, for the 3D media. $N(l)$ is the number of the eigenfrequencies in the interval l. In Fig. 9 the number variance is plotted for two frequency windows. For high frequencies the number variance is close to that of the Poisson distribution, whereas for low frequencies it behaves as the GOE statistics. These are in agreement with the results presented earlier.

B. Variance σ_s^2

To locate the transition point we also studied the variance,[35] σ_s^2 of $P(s)$,

$$\sigma_s^2=\langle s^2\rangle-\langle s\rangle^2=\int_0^\infty s^2P(s)ds-1. \tag{10}$$

Here, $\langle\cdot\rangle$ denotes an ensemble average over the realization of the disorder. In the delocalized regime in which the level-spacing distribution is represented by the WD distribution, the variance is, $\sigma_s^2=4/\pi-1\approx0.27$, while in the localized regime it is described by the Poisson distribution with, $\sigma_s^2=1$. Figures 10 and 11 present the frequency dependence of the variance σ_s^2 in 2D and 3D, respectively. In the 2D media at low frequencies the variance σ_s^2 is smaller than $2/\pi-1\simeq0.27$, indicating essentially the ballistic regime [in the completely ballistic regime with $P(s)=\delta(s-1)$, $\sigma_s^2=0$]. Figure 10 also demonstrates that in the 2D media of finite sizes, there exist crossovers between the three different regimes, namely, the ballistic, diffusive, and localized regimes.

The scaling behavior of level-statistics distribution was also studied. If the value of the variance σ_s^2 becomes closer to that of the delocalized (localized) states, as the size of the medium increases, the system is in the delocalized (local-

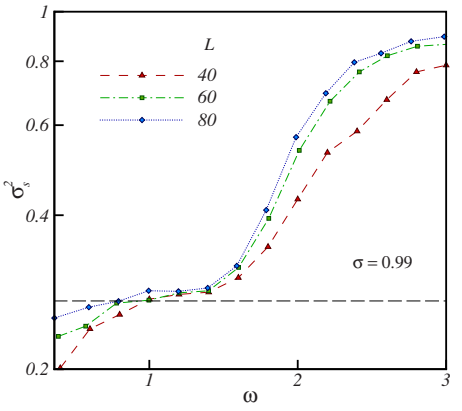

FIG. 10. (Color online) The variance σ_s^2 versus the frequency for sizes $L=40$, 60, and 80 of the 2D media, averaged over 800, 500, and 200 realizations of the disorder, respectively. The dashed line represents, $\sigma_s^2\simeq0.27$, the variance of the GOE. The low frequencies are in the ballistic regime and with a variance less than 0.27.

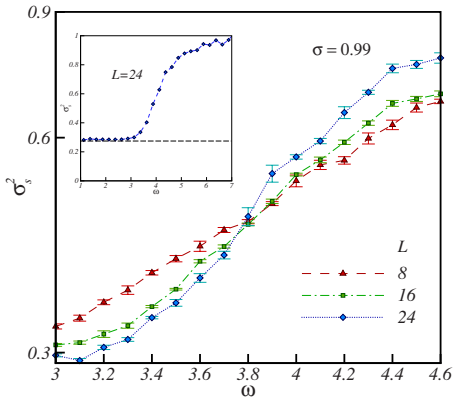

FIG. 11. (Color online) The variance σ_s^2 versus the frequency for 3D media of sizes $L=8$, 16, and 24, averaged, respectively, over 200 realizations of the disorder. Here, there is a critical frequency, $\omega_c \simeq 3.8 \pm 0.1$ at which the variance remains unchanged if the system's size increases. In the inset, the variance is plotted for a wide range of the frequencies. The dashed line represents, $\sigma_s^2 \simeq 0.27$, the variance of the GOE distribution.

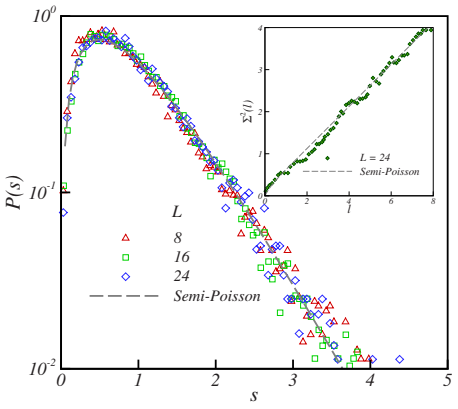

FIG. 12. (Color online) Logarithmic-linear plot of the level statistics in the critical frequency range, $3.7<\omega<3.9$, for three sizes of the 3D media. As shown, $P(s)$ is fitted well by the semi-Poisson distribution and is not sensitive to the size L. The inset shows that the number variance for the same critical frequency window, which is in good agreement with semi-Poisson distribution.

ized) regime.[31,35] Figure 10 indicates that, by increasing the size of the 2D media, the variance also increases. As the size of the media increases, the variances at low frequencies that correspond to the ballistic regime would be closer to those of the diffusive regime, whereas those in the latter regime go over the localized states.[37]

However, as Fig. 11 indicates for the 3D media, the finite-size scaling of the variance σ_s^2 has two distinct scalings, when the media's size (or volume) increases. The critical frequency ω_c at which the transition from one regime to the other occurs is deduced from the finite-size scaling analysis. We found that, $\omega_c \simeq 3.8 \pm 0.1$, which is in good agreement with the result of TM method, $\omega_c \simeq 3.7 \pm 0.1$.

C. Critical distribution

The scaling theory[38] predicts that, at the localization-delocalization transition frequency in 3D, the distribution function of the level spacings is *independent* of the system size. The distribution is represented well by the semi-Poisson distribution, $P(s)=4s\exp(-2s)$, and has the combined typical properties of both the localized and delocalized regimes. The level repulsion part of the distribution for small s, namely, $P(s) \propto s$, is similar to that of the WD distribution (the GOE universality class with $\beta=1$), while its exponential decay for large s is similar to that of the Poisson distribution.[28,38]

Figure 12 presents the dependence of $P(s)$ for three sizes of a 3D medium in the frequency window near the critical frequency, which was calculated by finite-size scaling of the variance. The results indicate that for all the sizes the level statistics is well fitted by the semi-Poisson distribution and, therefore, it is scale invariant. The inset of Fig. 12 shows the plot of number variance for the same critical frequency window, and is in good agreement with the number variance function, $\Sigma^2(l)=\frac{l}{2}+\frac{1}{8}(1-e^{-4l})$ for GOE model.

VII. SUMMARY

The localization properties of electromagnetic waves in 2D and 3D disordered medium were studied. Using the TM method and finite-size scaling, we showed that there is a localization-delocalization transition in disordered 3D media, for which we computed the mobility edge. We showed that 2D model for the s-polarized wave can be mapped onto the 2D Anderson model. For the 3D electromagnetic waves the critical exponent ν that characterizes the power-law behavior of the localization length near the transition point is the same as that of the 3D Anderson model.

The statistical properties of the energy levels have distinct distributions over different frequency ranges, hence indicating, in agreement with the TM results for the 3D media, the existence of the localization-delocalization transition. The statistical distribution of the energy levels for electromagnetic model behaves similarly too, and is in the universality class of the Gaussian orthogonal ensemble.

*moe@iran.usc.edu

[1] P. Sheng, *Introduction to Wave Scattering, Localization and Mesoscopic Phenomena* (Academic, San Diego, 1995).
[2] N. F. Mott and W. D. Twose, Adv. Phys. **10**, 107 (1961).
[3] I. Gol'dshtein, S. Molchanov, and L. Pastur, Funct. Anal. Appl. **11**, 1 (1977).
[4] S. Chandrasekhar, *Radiative Transfer* (Dover, New York, 1960).
[5] H. C. van de Hulst, *Multiple Light Scattering* (Academic, New York, 1980) Vols. 1 and 2.
[6] A. Lagendijk, in *Current Trends in Optics*, edited by J. C. Dainty (Academic, London, 1994).
[7] P. W. Anderson, Phys. Rev. **109**, 1492 (1958).

[8] D. S. Wiersma, P. Bartolini, A. Lagendijk, and R. Righini, Nature (London) **390**, 671 (1997); A. A. Chabanov, Z. Q. Zhang, and A. Z. Genack, Phys. Rev. Lett. **90**, 203903 (2003); P. M. Johnson, A. Imhof, B. P. J. Bret, J. G. Rivas, and A. Lagendijk, Phys. Rev. E **68**, 016604 (2003).
[9] M. V. Berry and S. Klein, Eur. J. Phys. **18**, 222 (1997).
[10] A. A. Chabanov, M. Stoytchev, and A. Z. Genack, Nature (London) **404**, 850 (2000).
[11] M. Storzer, P. Gross, C. M. Aegerter, and G. Maret, Phys. Rev. Lett. **96**, 063904 (2006).
[12] M. P. Van Albada and A. Lagendijk, Phys. Rev. Lett. **55**, 2692 (1985).
[13] P. E. Wolf and G. Maret, Phys. Rev. Lett. **55**, 2696 (1985).
[14] E. Akkermans, P. E. Wolf, and R. Maynard, Phys. Rev. Lett. **56**, 1471 (1986).
[15] F. Reil and J. E. Thomas, Phys. Rev. Lett. **95**, 143903 (2005).
[16] P. W. Anderson, Philos. Mag. B **52**, 505 (1985).
[17] A. A. Asatryan, L. C. Botten, M. A. Byrne, R. C. McPhedran, and C. M. de Sterke, Phys. Rev. E **75**, 015601(R) (2007).
[18] A. F. Ioffe and A. R. Regel, Prog. Semicond. **4**, 237 (1960).
[19] D. J. Thouless, Phys. Rep. **13**, 93 (1974).
[20] V. I. Oseledec, Trans. Mosc. Math. Soc. **19**, 197 (1968).
[21] E. P. Wigner, Proc. Cambridge Philos. Soc. **47**, 790 (1951).
[22] K. Efetov, *Supersymmetry in Disorder and Chaos* (Cambridge University Press, Cambridge, England, 1999); K. Efetov Cuevas, arXiv:cond-mat/0502322 (unpublished).
[23] O. Bohigas, M. J. Giannoni, and C. Schmit, Phys. Rev. Lett. **52**, 1 (1984); M. L. Mehta, *Random Matrices*, 3rd ed. (Elsevier, Amsterdam, 2004).
[24] S. E. Skipetrov and B. A. van Tiggelen, Phys. Rev. Lett. **96**, 043902 (2006).
[25] K. L. van der Molen, R. W. Tjerkstra, A. P. Mosk, and A. Lagendijk, Phys. Rev. Lett. **98**, 143901 (2007).
[26] A. Taflov and S. C. Hagness, *Computational Electrodynamics: The Finite-difference Time-Domain Method*, 3rd ed. (Artech House, New York, 2000).
[27] X. Li, A. Taflove, and V. Backman, Phys. Rev. E **75**, 037601 (2007); see also, A. Ishimaru, *Wave Propagation and Scattering in Random Media* (Academic Press, New York, 1978).
[28] P. Markos, Acta Phys. Slov. **56**, 561 (2006).
[29] R. A. Römer and H. Schulz-Baldes, Europhys. Lett. **68**, 247 (2004).
[30] E. Abrahams, P. W. Anderson, D. C. Licciardello, and T. V. Ramakrishnan, Phys. Rev. Lett. **42**, 673 (1979).
[31] B. Kramer and A. Mackinnon, Rep. Prog. Phys. **56**, 1469 (1993).
[32] K. Slevin and T. Ohtsuki, Phys. Rev. Lett. **82**, 382 (1999); T. Kawarabayashiy, B. Kramer, and T. Ohtsuki, J. Phys.: Condens. Matter **10**, 11547 (1998).
[33] R. Sepehrinia, M. R. Rahimi Tabar, and M. Sahimi, Phys. Rev. B **78**, 024207 (2008).
[34] K. Yakubo and T. Nakayama, Phys. Rev. B **40**, 517 (1989); K. Yakubo, T. Nakayama, and H. J. Maris, J. Phys. Soc. Jpn. **60**, 3249 (1991); K. Yakubo, K. Takasugi, and T. Nakayama, *ibid.* **59**, 1909 (1990); T. Nakayama and K. Yakubo, Phys. Rep. **349**, 239 (2001); M. Sahimi, *Heterogeneous Materials I* (Springer, New York, 2003), Chaps. 6 and 9.
[35] A. M. Garcia-Garcia and E. Cuevas, Phys. Rev. B **79**, 073104 (2009).
[36] V. E. Kravtsov and K. A. Muttalib, Phys. Rev. Lett. **79**, 1913 (1997); A. M. Garcia-Garcia and J. Wang, Acta Phys. Pol. A **112**, 635 (2007).
[37] B. I. Shklovskii, B. Shapiro, B. R. Sears, P. Lambrianides, and H. B. Shore, Phys. Rev. B **47**, 11487 (1993).
[38] A. M. Garcia-Garcia, Phys. Rev. Lett. **100**, 076404 (2008).